


**Realization of a quantum degenerate mixture of highly magnetic and nonmagnetic atoms**F. Schäfer<sup>✉,\*</sup>, Y. Haruna, and Y. Takahashi<sup>✉,†</sup>*Department of Physics, Graduate School of Science, Kyoto University, Kyoto 606-8502, Japan* (Received 18 January 2023; accepted 17 March 2023; published 29 March 2023)

We report on the experimental realization of a bosonic quantum degenerate mixture of highly magnetic  $^{168}\text{Er}$  and nonmagnetic  $^{174}\text{Yb}$ . Quantum degeneracy is reached by forced evaporation in an all-optical trap. Formation of the two Bose-Einstein condensates is confirmed by analysis of the cloud shape and the observed inversions of the aspect ratios. The results open a path for possible new experiments on magnetic and nonmagnetic impurity physics as well as on the quantum chaotic behavior of Feshbach resonances and their dependencies on minor variations of the reduced masses.

DOI: [10.1103/PhysRevA.107.L031306](https://doi.org/10.1103/PhysRevA.107.L031306)**I. INTRODUCTION**

The research field of ultracold atoms has become a vast and rich one. The number of atomic species that have been brought to quantum degeneracy spans across the entire periodic table of elements, reaching from the lightest ones [1] to very heavy species [2], and is by now too large to list them all individually here. In addition to single-species experiments, two-element experiments have also gained considerable attention. Starting with an ultracold Cs-Li mixture [3], this field also evolved in many directions, again covering a range from large-mass-imbalance Yb-Li mixtures [4] to highly magnetic and anisotropic Er-Dy mixtures [5]. This diversity is not redundancy but a richness of possibilities, each one looking at the fundamental questions stemming from quantum physics, many-body physics, quantum simulation, and quantum computation at slightly angles.

It is in this spirit that we here introduce another member to the family of experimentally realized quantum degenerate mixtures: a mixture of bosonic erbium ( $^{168}\text{Er}$ ) and bosonic ytterbium ( $^{174}\text{Yb}$ ). Without going to the extremes of either large mass imbalances or nearly overwhelmingly complicated interspecies interaction potentials, this mixture might be ideal for exploring physical phenomena in-depth and systematically with reasonable computational efforts, as first proposed and theoretically described by Kosicki, Borkowski, and Żuchowski [6]. In short, while quantum chaotic behavior could be confirmed experimentally in, e.g., the complex dynamics of highly magnetic and highly anisotropic Er-Er collisions [7], it is believed that evidence of quantum chaos may also be found in the significantly simpler Er-Yb collisional system. In that case, one of the collisional partners, Yb, is a comparatively-easy-to-model spin-singlet atom, and the interspecies interactions can be derived from *ab initio* calculations [6]. This greatly helps in identifying the driving mechanisms, such as anisotropic interactions, that contribute

to the chaotic behavior. Furthermore, as the two species have similarly large masses while also offering various isotopes each for use in the experiments, Er-Yb mixtures offer a unique possibility to study the effects of minute reduced-mass differences on the Feshbach spectra. The expected shifts of the interspecies Feshbach resonance positions should be well controlled and might be sensitive to temporal changes in the proton-to-electron mass ratio [8].

In addition, this quantum degenerate mixture is unique in that one of its constituents is a highly magnetic atom,  $^{168}\text{Er}$ , with a magnetic moment of  $7 \mu_B$  whereas the other one,  $^{174}\text{Yb}$ , is nonmagnetic. This offers the possibility of studying the magnetic-nonmagnetic impurity problem at vanishing interspecies interactions by means of a Feshbach resonance, especially when loaded into an optical lattice. There, the additional existence of narrow and ultranarrow optical transitions for both Er [9] and Yb [10] would provide a powerful tool for such investigations.

In the following we will first describe the details of our experiment relevant to the formation of the quantum degenerate  $^{168}\text{Er}$ - $^{174}\text{Yb}$  mixture (Sec. II). We then present the experimental data and our evidence for achieving simultaneous Bose-Einstein condensates (BECs; Sec. III) and conclude with a short discussion of these results (Sec. IV).

**II. EXPERIMENT**

The setup of the experiment and the experimental sequence are largely as in our previous works [11], and we will here only highlight the key aspects and changes relevant to the present work. After first loading the  $^{174}\text{Yb}$  magneto-optical trap (MOT) to saturation in 45 s a rather small amount of  $^{168}\text{Er}$  is added with just 2 s of loading. Due to the narrow-linewidth nature of the Er MOT the obtained Er sample is automatically spin polarized into the lowest-energy  $m_J = -6$  state [7,11]. Both species are then transferred into an optical far-off resonant trap in the horizontal direction (H-FORT) at 1064 nm where we typically obtain about  $3 \times 10^5$  Er atoms and  $4 \times 10^6$  Yb atoms, both at an estimated temperature of 80  $\mu\text{K}$ . This one-order-of-magnitude difference in atom

\*schaefer@scphys.kyoto-u.ac.jp

†takahashi.yoshiro.7v@kyoto-u.ac.jp

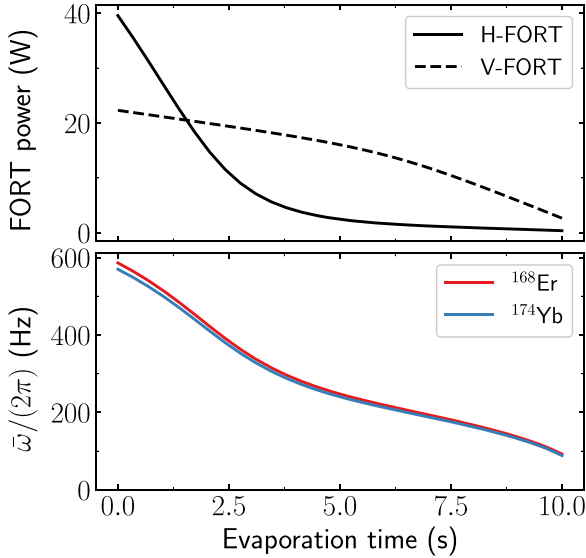


FIG. 1. Trap laser powers and trap frequencies during the forced evaporation process. Top: The evaporation in the two crossed FORT lasers requires 10 s. During that time the power of the H-FORT (solid line) is gradually decreased from roughly 40 to 0.4 W at the atoms. The V-FORT (dashed line) is for better lateral confinement initially kept closer to the initial power of about 22 W and then reduced to about 2.7 W. Bottom: The calculated geometric mean trap frequencies for Er (upper, red line) and Yb (lower, blue line). Due to the similar masses and polarizabilities the trap frequencies are quite similar. The trap frequencies show a nearly linear reduction in time, a surprising result of the independent evaporation ramp optimization that maximized the Yb BEC production efficiency.

numbers is to facilitate the sympathetic cooling of Er by Yb which this experiment relies on. That is, by forced evaporation of Yb the Yb sample has to not only cool itself down but also remove the energy from the Er sample which is in good thermal contact with Yb by means of frequent elastic collisions. Before evaporation a second FORT beam in the vertical direction (V-FORT) at 1070 nm is added for increased atom densities and thus evaporation efficiencies in the resulting crossed FORT configuration. In the following forced evaporation step, both FORT powers are gradually reduced over a period of 10 s as shown in the top panel of Fig. 1.

The evaporation ramp shape of each FORT is a spline curve with, in addition to the start and end points, two additional in-between control points. The ramp shapes and their duration have been optimized for optimal evaporation of  $^{174}\text{Yb}$ . During the first 4 s of evaporation a magnetic bias field of 1.6 G is applied in the vertical direction that is then reduced to 0.4 G for the remainder of the evaporation ramp. This choice is to ensure that the initial spin polarization of  $^{168}\text{Er}$  is maintained throughout the evaporation while also having optimal interspecies collisional properties and low Er-Er inelastic collisional losses [7].

Due to both the similar masses of  $^{168}\text{Er}$  and  $^{174}\text{Yb}$  and the similar polarizabilities of the two species at the wavelengths of the FORT lasers the resulting traps are quite similar. As expressed in the bottom panel of Fig. 1 the geometric mean trap frequencies start at about  $2\pi \times 600$  Hz and then decrease in a nearly linear fashion to about  $2\pi \times 100$  Hz

after 10 s. The final trap frequencies are about  $(\omega_x, \omega_y, \omega_z) = 2\pi \times (55, 70, 190)$  Hz, where  $\omega_z$  is in the vertical direction. From earlier works it is known that the  $^{174}\text{Yb}$ - $^{174}\text{Yb}$  scattering length is  $105 a_0$ , where  $a_0$  is the Bohr radius [12]. The  $^{168}\text{Er}$ - $^{168}\text{Er}$  scattering length was measured to be between 150 and 200  $a_0$ , where, however, additional effects due to dipole-dipole interactions should also be considered carefully [13]. The  $^{168}\text{Er}$ - $^{174}\text{Yb}$  interspecies scattering length is as of yet unknown.

### III. RESULTS

We now address the development of the atom numbers  $N$ , the temperatures  $T$ , and the phase-space density (PSD) during the evaporation process, which is shown in Fig. 2. As expected, at the expense of mostly Yb atoms the overall temperature of the mixture decreases. It is important to note the high fidelity with which the temperature of Er follows the temperature of Yb, highlighting the very good thermal contact between the two species and allowing for successful sympathetic cooling of Er. Correspondingly, the PSD increases by more than four orders of magnitude. After about 9.5 s of evaporation it reaches the critical value of about 2.6, the onset of quantum degeneracy into a BEC. This is further evidenced by the apparent discontinuity of the observed quantities at 10 s. This change is most probably due to the phase transition from a thermal cloud to a BEC where a Gaussian fit is no longer the appropriate description of the actual density distribution but instead highlights the sudden “compactification” of the sample.

As a measure of the evaporation efficiency we look at the relationship of the PSD, normalized to its initial value  $\text{PSD}_0$ , to the atom numbers  $N$ , normalized to their initial values  $N_0$ . There, usually a power-law-like behavior is observed, and  $\gamma = -d \ln(\text{PSD}/\text{PSD}_0)/d \ln(N/N_0)$  serves as a good indicator of evaporation efficiency [8]. In the case at hand (see Fig. 3), one obtains  $\gamma = 4.8(3)$  for Er and  $2.4(2)$  for Yb. Comparing this, e.g., with our earlier results in the evaporation of an Yb-Li mixture [14], we find a similar efficiency for Yb to that found before ( $\gamma_{\text{Yb}} = 2.9$  for Yb-Li) but a reduced evaporation efficiency of the sympathetically cooled species Er as compared with Li ( $\gamma_{\text{Li}} = 6.5$  in Yb-Li). This might in part be due to the reduced effect of gravity on the very light Li resulting in a significantly deeper trap and reduced losses for hotter Li atoms. The sympathetic cooling of Er is not perfect in the sense that a reduction in the Er atom number is also observed. It is rather that in this scenario of similar trap depths for both species and also due to favorable Er-Er collisional properties [13], Yb efficiently supports the cooling process of Er. This is further evidenced by the fact that in our experiment no Er BEC can be achieved by single-species evaporation due to an insufficient number of Er atoms initially loaded into the FORT, while a single-species-evaporated Yb BEC is possible.

We probe the dual-species BEC after 10 s of evaporation by standard absorption imaging. Before releasing the sample from the optical trap we keep the FORT lasers at their final values for an additional 500 ms to allow for final thermalization of the two atom clouds. The trapping lasers are then suddenly switched off, and the atoms are allowed to expand freely. After 22 ms of expansion time both atomic species are

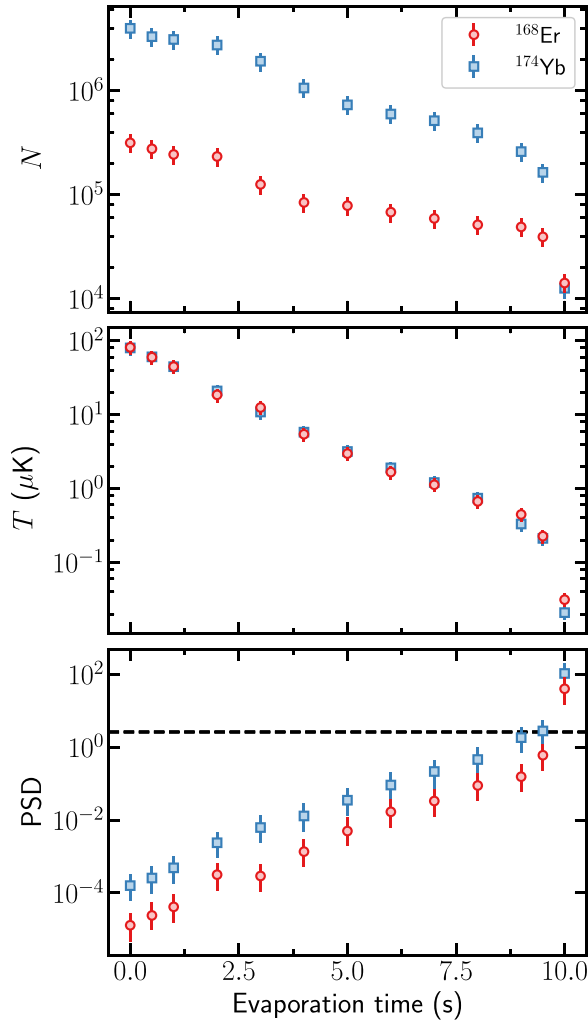


FIG. 2. Development of atom numbers (top), temperatures (middle), and phase-space densities (bottom) during evaporation of the  $^{168}\text{Er}$ - $^{174}\text{Yb}$  mixture. Initially, about one order of magnitude more Yb is loaded into the crossed FORT as it serves as the main coolant of the mixture. The close agreement of the Er and Yb temperatures demonstrates a very efficient interspecies thermalization dynamics, a necessary prerequisite for efficient sympathetic cooling of Er by Yb. Double quantum degeneracy of the sample is reached close to the end of the evaporation ramp where the phase-space densities rise above the critical threshold value of about 2.6 (black dashed line in bottom panel). The data points are averages over typically six independent renditions of the experiment, and the error bars take the uncertainties in the atom number and temperature determinations as well as the estimated possible errors in the assumed trap frequencies into account. See the main text for additional comments on the data at 10 s.

imaged simultaneously in absorption imaging on the strong transitions at 401 nm for Er and 399 nm for Yb. The results are shown in Fig. 4. Both clouds are reasonably well described by Thomas-Fermi distributions, indicative of only small contributions from still thermal atoms. Indeed, tentative fits with bimodal distributions (i.e., distributions including Gaussian-shaped thermal contributions) seemed unrealistic, a situation typically experienced in the case of only small thermal contributions. We find no appreciable change in the cloud shapes in

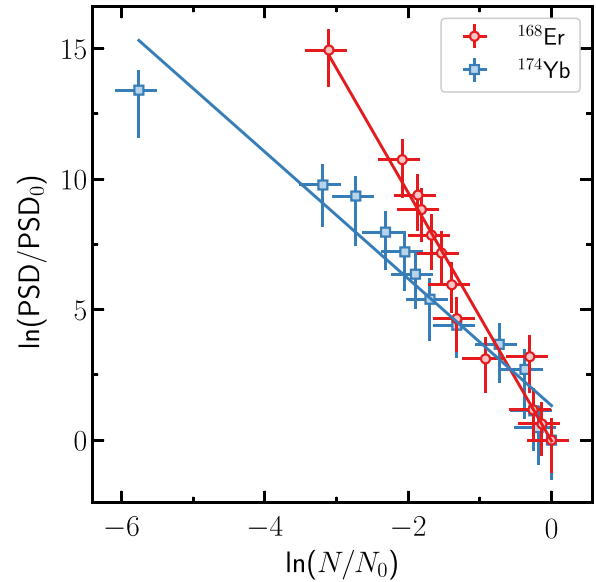


FIG. 3. Development of the normalized phase-space densities ( $\text{PSD}/\text{PSD}_0$ ) and the normalized atom numbers ( $N/N_0$ ) during evaporation.  $\text{PSD}_0$  and  $N_0$  are the respective values at the beginning of the evaporation ramp. The error bars account for uncertainties in the cloud and trap parameters. The trajectories for  $^{168}\text{Er}$  (red circles) and  $^{174}\text{Yb}$  (blue squares) can be approximately described and fitted by power laws (straight lines) with exponents of  $-4.8(3)$  for Er and  $-2.4(2)$  for Yb. The apparent twofold more efficient evaporation of Er is clearly due to the efficient sympathetic cooling by Yb.

the case where one species is removed before releasing the remaining atoms from the trap. This indicates that the Er-Yb interspecies interactions are below the threshold beyond which immiscibility effects are expected [15,16] and gives us the possibility to estimate an upper bound [17] for the Er-Yb scattering length,  $a_{\text{ErYb}}$ . Assuming an  $^{168}\text{Er}$  scattering length of  $a_{\text{Er}} \leq 200 a_0$  and taking the known  $a_{\text{Yb}} = 105 a_0$ , it follows that  $|a_{\text{ErYb}}| < 145 a_0$ .

The overall shape of the atom clouds in Fig. 4 is not spherically symmetric as would be expected of thermal samples. Instead they are elongated in the vertical direction. A more systematic investigation of the dependence of these aspect ratios on the expansion time is presented in Fig. 5, where expansion times in the range 0–18 ms are investigated. For both species an inversion of the aspect ratio at about 5–6 ms of expansion time is observed. This agrees reasonably well with a theoretically expected inversion point at about 4 ms based on the final trapping frequencies [18] and further corroborates the quantum degenerate nature of the ultracold mixture of  $^{168}\text{Er}$  and  $^{174}\text{Yb}$ .

Evaluating the stability of the obtained BEC mixture at 0.4 G, we observe lifetimes of the Er BEC in excess of 10 s while the lifetime of our Yb BEC is generally lower, at about 2 s, which is purely due to technical limitations of our apparatus and not due to the presence of Er. Therefore, for a more qualitative evaluation of the inelastic collisional processes, we investigate the atom loss with a cold but still thermal mixture at about 400 nK. There, we find single-species three-body collision rates [19] for  $^{168}\text{Er}$  and  $^{174}\text{Yb}$  of  $3(1) \times 10^{-28}$  and  $1.0(5) \times 10^{-28} \text{ cm}^6 \text{ s}^{-1}$ , respectively. The addition-

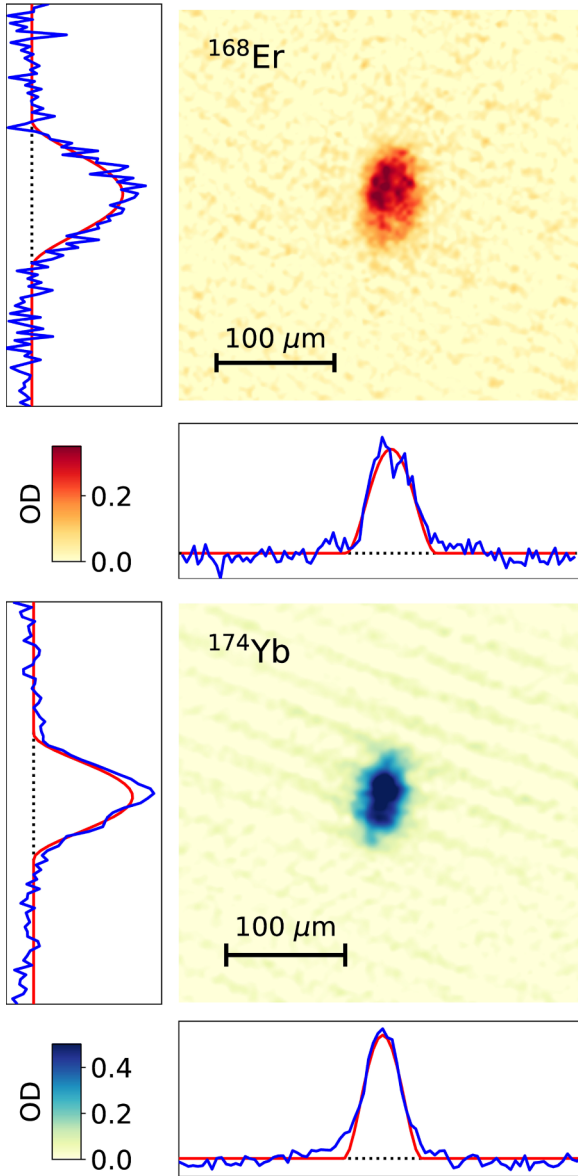


FIG. 4. Absorption images of  $^{168}\text{Er}$  (top panel) and  $^{174}\text{Yb}$  (bottom panel) Bose-Einstein condensates. Both images are the averages of 12 independent realizations of the experiment with absorption imaging after 22 ms of free expansion for both species. The colors indicate the recorded optical density (OD; see color bars). The additional graphs are the integrated column densities (ordinates are in a linear arbitrary units scale) of the data (blue) together with the fit results of Thomas-Fermi distributions (red). Even though the samples appear to be not fully quantum degenerate, the remaining thermal fractions are too low for reliable fitting with bimodal Thomas-Fermi-Gaussian distributions. The available fits indicate that there are about  $1.3 \times 10^4$  Er atoms and  $1.5 \times 10^4$  Yb atoms present in the final mixture.

ally observed interspecies three-body collisional losses are at  $1.0(5) \times 10^{-28} \text{ cm}^6 \text{ s}^{-1}$  comparable to the intraspecies losses and well described by Er-Yb-Yb interactions, while Er-Er-Yb collisions are not compatible with our observations. These low losses underline the good suitability of ultracold  $^{168}\text{Er}$ - $^{174}\text{Yb}$  mixtures for future experiments.

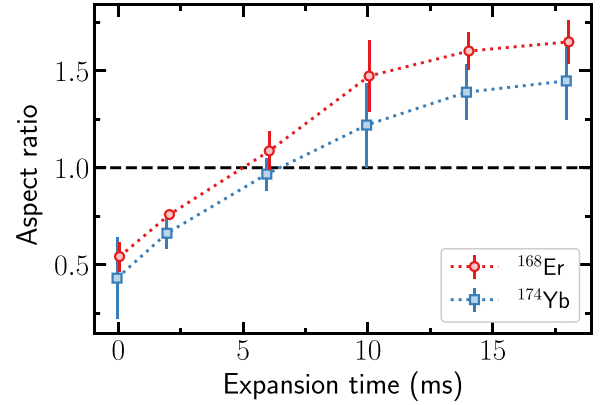


FIG. 5. Development of the cloud aspect ratios for Er (red circles) and Yb (blue squares) during different expansion times. The aspect ratio is here defined as the ratio of cloud height over cloud width. It follows that at short expansion times the clouds still maintain their in-trap shape. After 5–6 ms the anisotropic expansion due to the stored interaction energy causes both clouds to become elongated in the vertical direction. This inversion of the aspect ratio is a hallmark feature of BECs that cannot be observed with thermal clouds. The dashed lines are intended as a guide to the eye.

#### IV. DISCUSSION

First and foremost the work presented here confirms that a stable formation of a  $^{168}\text{Er}$ - $^{174}\text{Yb}$  double BEC is not only theoretically desirable but also experimentally feasible. That is by no means an *a priori* certainty as the expected dense interspecies Feshbach resonance structure might easily have interdicted such a state by strong inelastic collisional losses at the low magnetic fields that are typically used during standard evaporation stages. Along the way, our experiment once again underlines the quite amazing versatility of the heavy Yb not only from a physics standpoint but also in its capability to efficiently cool a variety of other species sympathetically [4,11].

The present work focused on the most commonly used bosonic isotopes of Er and Yb. An extension to different isotope combinations with interesting applications to fundamental research [6] appears straightforward, and our experiment is already set up to also work with various bosonic and fermionic isotopes.

It seems obvious that from these encouraging results it is only a few minor steps towards a full investigation of the  $^{168}\text{Er}$ - $^{174}\text{Yb}$  interspecies Feshbach resonance spectrum for at least this isotope combination. In the case of our experiment, in particular, we will, however, need to first make some improvements to (i) increase the atoms numbers in the final ultracold samples and (ii) improve the magnetic field stability of our setup [11]. The latter will be necessary to reliably identify also the narrow Feshbach resonances in order to obtain complete Feshbach spectra that are necessary for the envisioned statistical analyses. These instrumental challenges are not insurmountable, and we are therefore confident that our results will further enrich the family of experiment-proven ultracold atomic mixtures to address some of the quantum questions of our times.

## ACKNOWLEDGMENTS

This work was supported by the Grant-in-Aid for Scientific Research of JSPS Grants No. JP17H06138, No. 18H05405, and No. 18H05228, JST CREST Grant No. JPMJCR1673,

and the Impulsing Paradigm Change through Disruptive Technologies (ImPACT) program by the Cabinet Office, Government of Japan, and MEXT Quantum Leap Flagship Program (MEXT Q-LEAP) Grant No. JPMXS0118069021 and Moonshot Program Grant No. JPMJMS2269.

- 
- [1] D. G. Fried, T. C. Killian, L. Willmann, D. Landhuis, S. C. Moss, D. Kleppner, and T. J. Greytak, *Phys. Rev. Lett.* **81**, 3811 (1998).
- [2] Y. Takasu, K. Maki, K. Komori, T. Takano, K. Honda, M. Kumakura, T. Yabuzaki, and Y. Takahashi, *Phys. Rev. Lett.* **91**, 040404 (2003).
- [3] A. Mosk, S. Kraft, M. Mudrich, K. Singer, W. Wohlleben, R. Grimm, and M. Weidemüller, *Appl. Phys. B* **73**, 791 (2001).
- [4] A. H. Hansen, A. Khramov, W. H. Dowd, A. O. Jamison, V. V. Ivanov, and S. Gupta, *Phys. Rev. A* **84**, 011606(R) (2011).
- [5] A. Trautmann, P. Ilzhöfer, G. Durastante, C. Politi, M. Sohmen, M. Mark, and F. Ferlaino, *Phys. Rev. Lett.* **121**, 213601 (2018).
- [6] M. B. Kosicki, M. Borkowski, and P. S. Żuchowski, *New J. Phys.* **22**, 023024 (2020).
- [7] A. Frisch, M. Mark, K. Aikawa, F. Ferlaino, J. L. Bohn, C. Makrides, A. Petrov, and S. Kotochigova, *Nature (London)* **507**, 475 (2014).
- [8] W. Ketterle and N. V. Druten, in *Advances in Atomic, Molecular, and Optical Physics* (Academic, New York, 1996), Vol. 37, pp. 181–236.
- [9] A. Patscheider, B. Yang, G. Natale, D. Petter, L. Chomaz, M. J. Mark, G. Hovhannesian, M. Lepers, and F. Ferlaino, *Phys. Rev. Res.* **3**, 033256 (2021).
- [10] A. Yamaguchi, S. Uetake, S. Kato, H. Ito, and Y. Takahashi, *New J. Phys.* **12**, 103001 (2010).
- [11] F. Schäfer, N. Mizukami, and Y. Takahashi, *Phys. Rev. A* **105**, 012816 (2022).
- [12] M. Kitagawa, K. Enomoto, K. Kasa, Y. Takahashi, R. Ciuryło, P. Naidon, and P. S. Julienne, *Phys. Rev. A* **77**, 012719 (2008).
- [13] K. Aikawa, A. Frisch, M. Mark, S. Baier, A. Rietzler, R. Grimm, and F. Ferlaino, *Phys. Rev. Lett.* **108**, 210401 (2012).
- [14] F. Schäfer, N. Mizukami, P. Yu, S. Koibuchi, A. Bouscal, and Y. Takahashi, *Phys. Rev. A* **98**, 051602(R) (2018).
- [15] C. J. Pethick and H. Smith, *Bose-Einstein Condensation in Dilute Gases*, 2nd ed. (Cambridge University Press, Cambridge, 2008).
- [16] A. Burchianti, C. D’Errico, M. Prevedelli, L. Salasnich, F. Ancilotto, M. Modugno, F. Minardi, and C. Fort, *Condens. Matter* **5**, 21 (2020).
- [17] F. Riboli and M. Modugno, *Phys. Rev. A* **65**, 063614 (2002).
- [18] Y. Castin and R. Dum, *Phys. Rev. Lett.* **77**, 5315 (1996).
- [19] Z.-X. Ye, A. Canali, E. Soave, M. Kreyer, Y. Yudkin, C. Ravensbergen, E. Kirilov, and R. Grimm, *Phys. Rev. A* **106**, 043314 (2022).